S. BOGDANSKI *, J. STUPNICKI *, M. W. BROWN ** and
D. F. CANNON ***

A Two Dimensional Analysis of Mixed-Mode Rolling Contact Fatigue Crack Growth in Rails

* Institute of Aeronautics and Applied Mechanics, Warsaw University of Technology, Nowowiejska 22/24, 00-665 Warsaw, Poland.

** SIRIUS, Department of Mechanical Engineering, The University of Sheffield, Mappin Street, Sheffield, S1 3JD, U.K.

*** European Rail Research Institute, Utrecht, Netherlands.

Keywords: rolling contact, mixed-mode, non-proportional, crack growth, fluid entrapment

ABSTRACT: In rolling contact fatigue of rails, cracks form at a shallow angle, and grow primarily in the direction of travel underneath the rail surface. Once nucleated, cracks may branch to a mode I direction, whereas shallow cracks grow when the crack is filled with fluid. This paper attempts to model the response of shallow-angle cracks through fracture mechanics analysis, using finite element stress analysis and multiaxial fatigue tests to simulate the rolling contact history. The evolution of the history of mixed-mode I and II stress intensity factors is derived from a 2D finite element model. Biaxial fatigue crack propagation experiments have been conducted on BS11 rail steel to investigate the effect of sequential mixed-mode loading on angled cracks. The effects of fluid in the crack, residual stress in the rail head and braking are considered to demonstrate that "squat" rolling contact fatigue cracks can only develop under prescribed loading conditions.

Introduction

Over the last 20 years or so surface initiated rolling contact fatigue (RCF) has been increasingly observed on modern mixed traffic and high speed rail systems in countries with temperate climates. Rails made of pearlitic steels with hardness levels ranging from about 220 BHN to 380 BHN have experienced this type of fatigue damage. Once nucleated, typical cracks propagate at a shallow angle under the rail's running surface, primarily in the direction of vehicle travel. These cracks may branch either up or down; the former case leading mostly to surface spalling and the latter to predominantly mode I driven cracks lying close to the rail's transverse plane and, in the absence of corrective

maintenance action, rail fracture may occur. Shallow cracks appear to grow only when the crack is filled with fluid. It is also believed that residual stresses in the rail and wheel traction forces influence the response. This paper attempts to model the response of shallow-angle cracks through fracture mechanics analysis, using finite element stress analysis and multiaxial fatigue tests to simulate the rolling contact history. A satisfactory fatigue crack propagation prediction should model each of the above parameters.

The important role of liquid in creating the crack tip stress histories during cyclic contact loading has been discussed by Way (1), Keer and Bryant (2), Bower (3), Kaneta and Murakami (4) and Bogdanski et al. (5). It is widely believed that liquid can influence fatigue crack growth by reducing friction between crack faces, by pressure on the crack faces as fluid flows into the crack, and by the "fluid entrapment effect" exerting hydrostatic pressure at the crack tip. The entrapment mechanism, illustrated in Fig. 1, provides high levels of K_I due the hydraulic pressure opening the crack as the wheel rolls towards the crack tip. Frequently invoked in discussions of RCF in rails (5, 6, 7), fluid entrapment applies to bearings and gears also. It is assumed here that a liquid (e.g. rain water) present on the rail surface will be drawn into the crack during its initial opening, then entrapped during the subsequent phase of crack locking. Combining numerical stress analyses with experimental results provides a quantitative prediction of the fluid entrapment mechanism in terms of fatigue crack growth rate.

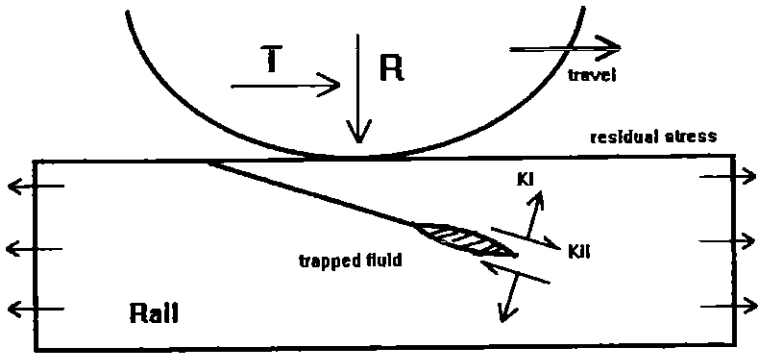

Fig. 1. A schematic of the fluid entrapment mechanism for RCF in railway lines.

Numerical modelling

The problem of rolling a wheel over a rail was modelled by three different methods. For the first method dry conditions were assumed, i.e. no liquid between the crack faces, which results in high friction. In the second and third ways liquid is present in the crack, but for the second case its only role is to lubricate the crack faces, which reduces the friction. The third way of modelling allows a certain volume of liquid to enter the crack interior in its initial phase of opening, becoming entrapped inside the crack during the phase of locking. A 2D plane strain finite element (FEM) model of a cylinder rolling over a prism (Fig. 2) has been incorporated in each analysis, with contact elements at the cylinder/prism interface and along the crack faces, distributed uniformly. The crack tip is surrounded by eight special triangular elements. Boundary conditions simulating the real rail/wheel contact system were assumed, i.e. the nodes located on the bottom face of the prism are fixed in the direction perpendicular to the prism longitudinal axis, whilst the side faces of the prism are fixed in the direction parallel to this axis (Fig. 2) Material properties for rail steel were modulus of elasticity E= 210 GPa and Poisson's ratio $\nu = 0.3$. All calculations, regardless of the version of modelling were carried out for the normal load R = 90 kN, and for the coefficient of friction at the cylinder/prism interface $\mu_S = 0.4$. Various friction coefficients μ_{CF} from 0.0 to 0.4 were taken for the crack faces, under wet or dry conditions respectively. Analyses included different traction loads and residual stresses occurring in rails in practice, to investigate their influence on the values and histories of the stress intensity factors (SIFs).

It was assumed in the first method that liquid is not present in the vicinity of crack, and hence the crack interior is free from liquid during the whole cycle of loading. Such conditions can occur in practice during sunny weather which dry the crack faces. This results in high friction between the crack faces under compressive contact loads, with an assumed coefficient of friction μ_{CF} of 0.4.

For the second method, it was assumed that a defined volume of liquid enters the crack, reducing friction between the crack faces. No other liquid action (exertion of pressure on the crack faces, or entrapment phenomena) was taken into account here. The third method is discussed in detail in the next section.

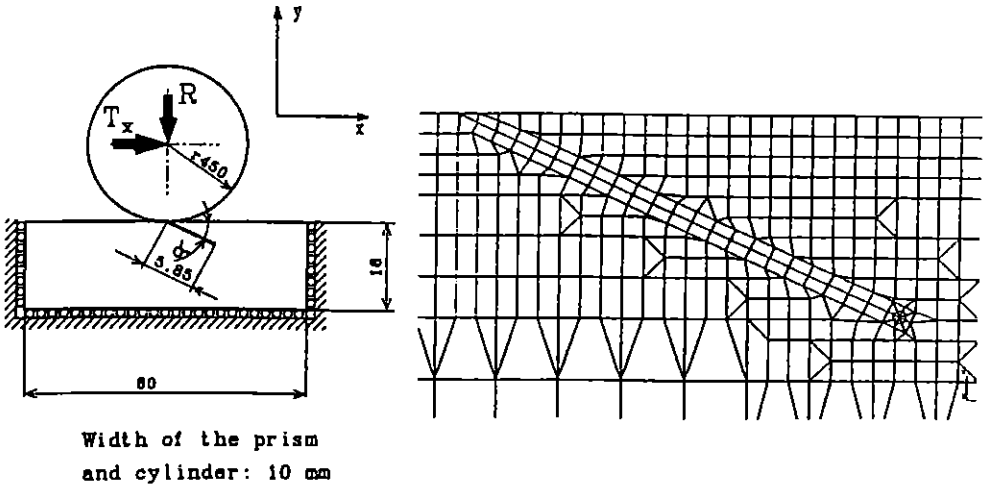

Fig. 2 The contact model, a) two- dimensional model of a rail / wheel contact system, b) non-deformed finite element mesh of the prism in the vicinity of crack, $\alpha = 25°$.

Wet conditions - liquid entrapped in the crack interior

The entire cycle of rolling the wheel over the crack can be divided into phases; the initial phase in which the crack is open, and the second phase where the crack mouth is locked. This differs from the second analysis above only in the second phase, where liquid is entrapped inside the crack. Loading progresses as follows. The crack gradually opens as the cylinder approaches, drawing liquid into the crack interior. The opening process lasts until the cylinder touches the opposite side of the crack mouth, i.e. the apex of a wedge-shaped prism situated above the crack plane (Fig. 3a).

Continued rolling of the cylinder causes the apex to bend downwards until it touches the lower crack face (Fig. 3b). In the lower part of the open crack the faces remain separated from each other, creating a locked space ("bubble") which is completely filled with a volume of incompressible liquid. Further analysis is performed in steps whilst the shape of the "bubble" and the pressure inside it are determined by the equilibrium conditions. The value of the gauge pressure at the starting point, i.e. at the moment of locking the

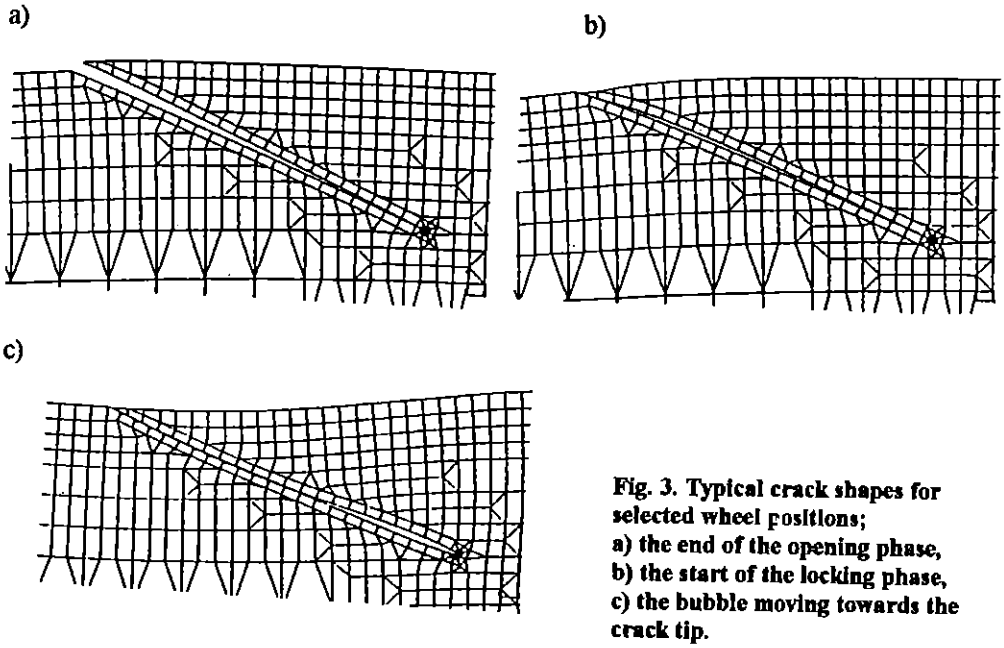

Fig. 3. Typical crack shapes for selected wheel positions;
a) the end of the opening phase,
b) the start of the locking phase,
c) the bubble moving towards the crack tip.

crack mouth, is taken as zero. Rolling of the cylinder causes the crack face stiction zone to spread towards the crack tip (Fig. 3c), accompanied by a gradual increase of fluid pressure. In addition, it was assumed that the pressure varies linearly along the stiction zone, i.e. the gauge pressure at the first pair of nodes in contact at the crack mouth is zero, whilst the pressure at the last pair is that of the entrapped liquid. The assumption of a linear pressure distribution relates to reality, where locking of the crack is not ideal due to the surface roughness, and hence liquid may leak slowly from the "bubble", reducing pressure along the flow path. This assumption allows estimation of upper bound SIFs, as any leakage reduces the "bubble" volume, lowering the mode I SIF values. For high speed trains, SIFs should approach the upper bound.

Mathematical model and solution

The mathematical model consists of the set of equilibrium equations which are written for every pair of contact nodes. A detailed description of the model used in the analysis, together with the procedure of solution, was presented in (8, 9). Taking into account the fluid entrapment effect required some modification to the previous model. The solution

to this problem leads to the sequential solution of a number of sets of equations written for the consecutive positions of the cylinder rolling over the crack, in increments of less than 0.01 mm. To ensure a reasonable accuracy of solution and stability of iteration procedure with fluid entrapment, it is necessary to apply a finer mesh in the contact zone compared to dry conditions. Before starting the main iteration procedure for solving the contact problem, the flexibility matrices for the cylinder and prism should be determined by FEM with the use of cylinder and prism finite element meshes. The iteration procedure for the analysis of the fluid entrapment effect required special care and attention, following preparatory calculations for dry conditions. The results obtained from these preliminary calculations were used as the initial data for the full analysis including the fluid entrapment effects.

Results of the SIF calculations

The purpose of this analysis was to investigate the influence of three parameters on the SIFs K_I and K_{II} and consequently on crack growth rate and direction, namely crack inclination angle, α, tangential longitudinal load, T_X (braking force), and rail residual stress, σ_T, acting separately or in combination. Plane strain calculations were carried out for dry, wet and fluid entrapment conditions for a wheel radius D/2 = 450 mm, normal load, R = 90 kN, three values of longitudinal load, T_X = 0, 9, 18 kN, and three values of residual stress, σ_T = -200, 0, +200 MPa. The numerical calculations determined the displacements, strains and stresses acting in the contact area of the cracked prism. The surface breaking cracks of length a = 5.85 mm (which is a/b = 0.87, where b = 6.7 mm is the semi-width of the contact patch) were inclined at the angles α = 15° and α = 25° to the surface of contact. The calculations were carried out for a cycle of loading covering the distance between x/b = - 2.5, and x/b = 3.3, where x is the distance of the contact patch from the crack mouth.

The comparison of the SIF histories obtained for all analysed cases yields the conclusion that the fluid entrapment mechanism has the greatest influence on the SIF ranges ΔK_{II} and ΔK_I developed during the loading cycle. Examples of the effect of this mechanism are presented in Fig. 4, showing K_I and K_{II} plotted versus the location of the wheel axis

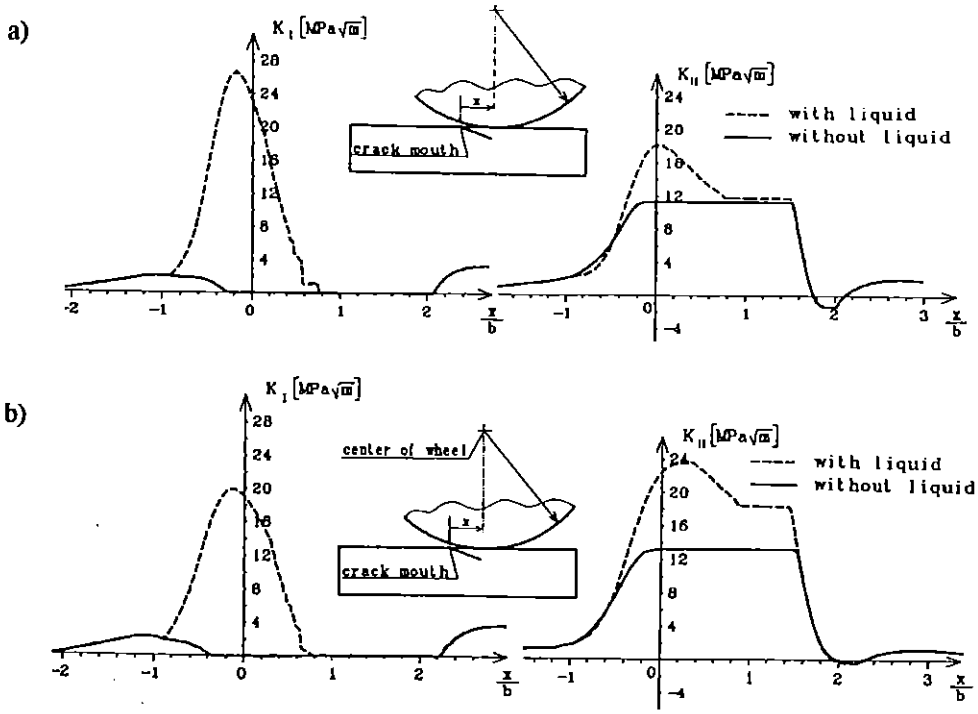

Fig. 4. Comparison of K_I and K_{II} histories as the wheel rolls over the crack with/without fluid entrapment. R= 90 kN, $T_x = 0$, $\sigma_{r.}=0$, $\mu_s = \mu_{cr.}=0.4$. a) $\alpha = 15°$, b) $\alpha = 25°$.

in relation to the crack mouth for two angles, $\alpha = 15°$ and $\alpha = 25°$. As shown, the factor influenced most by the liquid pressure is the SIF K_I, which increased by 660% and 470% for the cracks inclined at angles of 15° and 25°, respectively. Analysing the SIF histories for the example of $\alpha = 25°$, the following should be noticed. The SIF K_I increases sharply from the moment when the locked "bubble" of liquid develops ($x \approx -6$ mm), until it reaches the value about 20.0 MPa$\sqrt{m}$ ($x \approx -1.8$ mm). Then K_I decreases to zero when $x \approx 5.6$ mm as the liquid has completely drained out from the crack. The section of the K_{II} curve for fluid entrapment with $x > 5.6$ mm ($x/b \approx 0.8$) is similar to that obtained for dry conditions. The SIF K_{II} reaches a maximum of 24.0 MPa$\sqrt{m}$ at $x \approx 2.0$ mm, and then decreases as liquid drains from the crack interior ($x \approx 5.6$ mm). The SIF K_{II} is constant and equal 18.0 MPa$\sqrt{m}$ for the wheel positions of 5.6 mm $< x <$ 10.0 mm, due to interfacial crack friction. This constant K_{II} value is higher than that of the case without liquid, being equal to 13.0 MPa$\sqrt{m}$.

The characteristic shape of the SIF K_{II} history can be explained by analysing the phenomena which occur during the loading cycle. With intensive liquid flow out from the crack, the crack faces are separated by the liquid film and can slip easily against each other. Similarly though not so effective, when the crack is partially locked in the stiction zone, liquid flow through this zone is possible. As a result of this flow, the tangential forces that hinder slippage of the crack faces are reduced. Finally, the shear behaviour of the crack is as if it was empty but with a reduced friction coefficient, so that the shape of the section of the K_{II} curve for $-6.0 < x < 5.6$ mm is similar to the curve derived for the case with no liquid and no friction $\mu_{cr} = 0$.

Modelling of fatigue crack growth

The load history experienced by a crack in rolling contact fatigue can be simulated using a biaxial cruciform specimen, with independent control of the loads on each axis. Experimental results are available for mixed-mode fatigue crack propagation in normal grade BS11 rail steel, where 45^0 inclined cracks in cruciform specimens subject to characteristic tensile/shear load sequences (10, 11, 12) emulate the histories shown in Fig. 4. The results demonstrate that crack growth rate and direction are governed by the effective mode I and mode II SIF ranges. In rolling contact, an initial mode I cycle is experienced as the rail bends, or as fluid is pressurised. The SIF ΔK_{Inom} is simulated by equibiaxial tension: it is followed by a mode II cycle ΔK_{IInom} in pure shear (representing the contact patch passing over the crack tip). Generally the two waveforms may overlap. Mean stress is an additional factor that affects growth, which reflects the residual stress state in rail heads. Here ΔK_{Inom} and ΔK_{IInom} are the nominal mode I and II SIF ranges for experiments. Details of test methods and rail steel examined are given in (10, 11).
Bold (11) showed that when the ratio ΔK_{IInom} / ΔK_{Inom} was greater than 2, the crack branched to follow a mode I direction of maximum tangential stress. Thus, coplanar crack extension can be produced from this type of loading cycle with no waveform

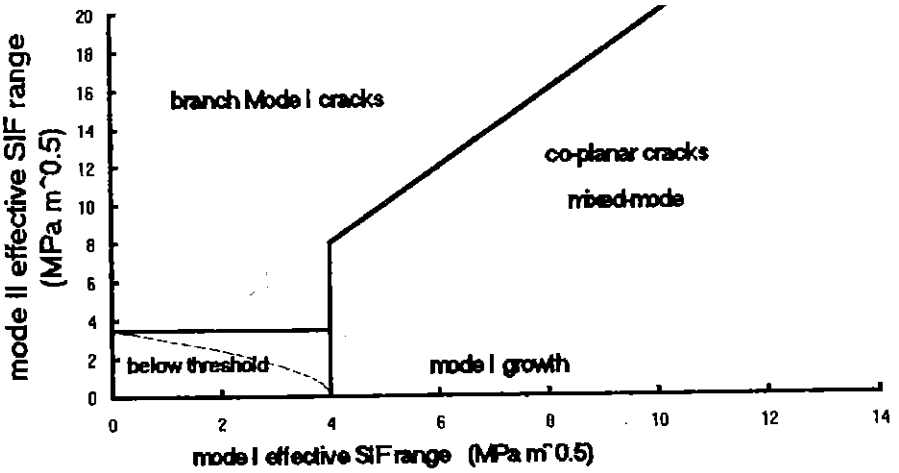

Figure 5. Three phases of fatigue crack growth under sequential mixed-mode loading.

overlap under a suitable combination of ΔK_{Inom} and ΔK_{IInom}, as shown in Fig. 5. (A coplanar crack on a 45° plane grows on a plane of maximum shear, whereas a mode I crack follows a principal direction.) However when the waveforms are in-phase (180° overlap) with the mode I and II peak SIFs occurring at the same time, initial shear mode defects in steels always deviate to become tensile mode I fatigue cracks, because the shear mode cannot be sustained.

When results are presented in terms of nominal ranges of stress intensity factor, the picture is complicated by crack closure and frictional effects. A clearer view is obtained in fatigue when effective ranges are used (Fig. 5), based on values of the crack closure load. In mode II shear, the corresponding concept is locking up of the fracture faces due to friction and wear. Whenever crack faces are in contact, both shear and normal stresses at the crack tip are attenuated, and consequently the fatigue damage is reduced. Figure 5 indicates three regions of propagation, a) branch mode I cracking, where rate and path are determined by the maximum tangential stress criterion, b) coplanar shear cracking on the 45^0 plane, which exhibits a characteristic very straight path due to the single slip system at the tip, and c) coplanar mode I cracking for small ΔK_{IInom}, which shows a more tortuous path due to the operation of twin crack tip slip bands (12). Finally there is a

threshold region, taken as a rectangular box for sequential loading after Lee (13), but following the curved shape for in-phase proportional stressing (14).

Effective measurements of the actual SIF ranges experienced by the crack tip were made in the tests. The effective mode I and mode II ranges, ΔK_{Ieff} and ΔK_{IIeff}, are defined as:

$$\Delta K_{Ieff} = U_I \Delta K_{Inom} = U_I Y \Delta\sigma \sqrt{\pi a} \quad (1)$$

$$\Delta K_{IIeff} = U_{II} \Delta K_{IInom} = U_{II} Y \Delta\tau \sqrt{\pi a} \quad (2)$$

where Y is the geometry factor for a central 45° crack of length 2a, and U_I and U_{II} are the proportions of applied load range or theoretical sliding displacement experienced by the crack tip, respectively.

Classical mode I fracture mechanics tests are characterised by three parameters, the range ΔK, the mean stress R ratio, and the closure ratio U_I, where $R = \sigma_{min} / \sigma_{max}$ is the conventional definition for R. For sequential loading in RCF, values for ΔK, R and U arise for the mode II cycle also. The waveforms overlap in Fig. 4, introducing a phase angle as a seventh control parameter. (In Fig. 6, the sinusoidal cycles employed always had R_I values of 0 and R_{II} values of -1, with various phase angles.) In practical situations cases, residual stresses may have a significant effect on RCF crack growth. Therefore, the effects of retaining some tension or compression through the shear cycle

Table 1. Mean stress and closure levels derived from numerical analysis.

α°	fluid	Tx kN	σ_r MPa	R_I	R_{II}	S_I	S_{II}	coplanar crack U_I	coplanar crack U_{II}	branch crack U_I	branch crack U_{II}
15	wet	0	-200	0.00	-0.83	0.00	-0.60	1.00	1.00	0.61	0.55
25	wet	0	-200	0.00	-0.75	0.00	-0.75	1.00	1.00	0.13	0.57
15	wet	0	0	0.00	-0.11	0.00	0.11	1.00	1.00	1.00	0.90
15	wet	18	0	0.00	-0.04	0.00	0.04	1.00	1.00	1.00	0.96
25	wet	0	0	0.00	-0.02	0.00	0.08	1.00	1.00	1.00	0.98
15	dry	0	-200	mode II	-3.20	mode II	-3.20	1.00	1.00	0.00	0.00
15	dry	18	-200	mode II	-10.00	mode II	-0.50	1.00	1.00	0.00	0.00
15	dry	0	0	0.00	-0.18	0.00	0.17	1.00	1.00	1.00	0.85
15	dry	18	0	0.00	0.00	0.00	0.00	1.00	1.00	1.00	1.00
25	dry	0	0	0.00	-0.04	0.00	0.17	1.00	1.00	1.00	0.96
15	dry	0	200	0.00	0.20	0.00	0.41	1.00	1.00	1.00	1.00
15	dry	18	200	0.00	0.33	0.00	0.33	1.00	1.00	1.00	1.00
25	dry	0	200	0.00	0.23	0.00	0.36	1.00	1.00	1.00	1.00

and retaining a static shear through the mode I cycle are important. Two further load parameters are defined as S ratios, where

$$S_I = K_{Idwell} / K_{Imax} \quad (3)$$

$$S_{II} = K_{IIdwell} / K_{IImax} \quad (4)$$

Here K_{Idwell} is the mean level of K_I during the mode II cycle, and vice versa. The value of S lies between R and unity. Thus to define a sequential load history with sinusoidal waveforms, nine independent parameters are required, the values for ΔK, R, S and U for modes I and II respectively, and the overlap angle, assuming that the cycles used are both sinusoidal. The values of characteristic parameters are given in Table 1, for the rolling contact analyses examined numerically.

Experimental crack growth results for sequential mixed-mode loads

Crack growth results are presented in Fig. 6 for normal grade BS11 rail steel, for the propagation of coplanar cracks. On the abscissa, the equivalent SIF plotted is $\Delta K_{eq} = \sqrt{\Delta K_I^2 + \Delta K_{II}^2}$, which is chosen purely as a convenient way to plot mode I and II data together. Results that relate to mode I like cracks (Fig. 5) fall round the upper bound line plotted, and those which resemble the straight mode II like cracks tend to the lower bound line. All data are contained within the factor of 2 scatter band shown as dotted lines. It is apparent that by using effective values of SIF, equations (1) and (2), data are bounded by the lines for the mode I and mode II mechanisms, irrespective of overlap angle and ratio of $\Delta K_{IInom} / \Delta K_{Inom}$, whose values are given in the key of Fig. 6.

A fatigue crack growth model can be postulated for mixed-mode sequential loading, to include the three mechanisms of propagation identified in Fig. 5. The Paris law describes coplanar mode I growth with an added threshold term, assuming an intrinsic threshold of 4 MPa$\sqrt{m}$ based on data for rail steel (15). Thus the upper bound line in Fig. 6 becomes

$$da / dN = 0.000507 (\Delta K_{eq}^{3.74} - 4^{3.74}) \quad \text{nm/cycle} \quad (5)$$

where the fitted constant and exponent were determined by Wong et al. (10) from mode I test data. For the mixed-mode coplanar mechanism, the lower bound line gives a second crack growth relationship, which corresponds to the shear mode law of Wong (12).

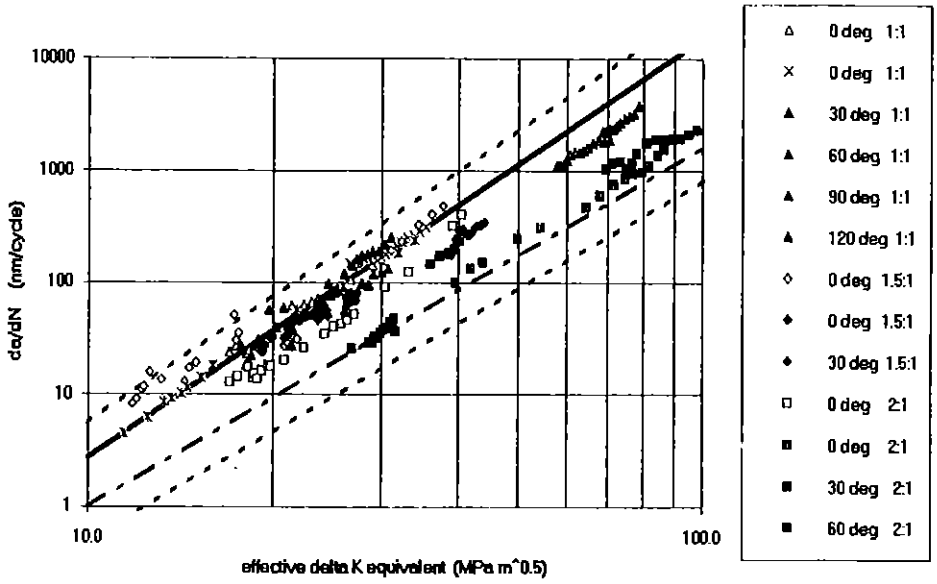

Figure 6. Coplanar fatigue crack growth under sequential mixed-mode loading for rail steel. The upper bound (solid line) is the Paris mode I law, and the lower bound (chain dot) is a mode II law. Key gives cycle overlap (in degrees) and ratio ΔK_{IInom} / ΔK_{Inom}.

When employing an equivalent SIF, $\Delta K_{eq} = \sqrt{\Delta K_I^2 + \Delta K_{II}^2}$, the shear mode rule becomes

$$da \ / \ dN = 0.000614(\Delta K_{eq}^{3.21} - 4^{3.21}) \qquad \text{nm/cycle} \qquad (6)$$

A non-linear weighting is proposed to interpolate between the two bounding solutions (16). Using the mode I Paris law for fatigue crack growth in equation (5), for coplanar propagation, an equivalent SIF range is defined such that

$$\Delta K_{eq}^2 = \Delta K_I^2 + [(614 \ / \ 507)\Delta K_{II}^{3.21}]^{2/3.74} \qquad (7)$$

In equations (5), (6) and (7), the SIFs are effective ranges. Equations (5) and (7) encompass both types of coplanar crack extension depicted in Fig. 5. All available coplanar propagation data are collated in Fig. 7 using the equivalent SIF of equation (7) in the mode I Paris law (equation (5)). Results fall broadly within a factor of 2 scatter band, except where the propagation rates fall off as a crack approaches a point of branching instability. The data include tests where R_I, R_{II}, S_I and S_{II} are investigated, as well as the previous results with overlap angle and mixed-mode ratio as parameters. The degree of correlation obtained suggests that equations (5) with (7) provide an effective

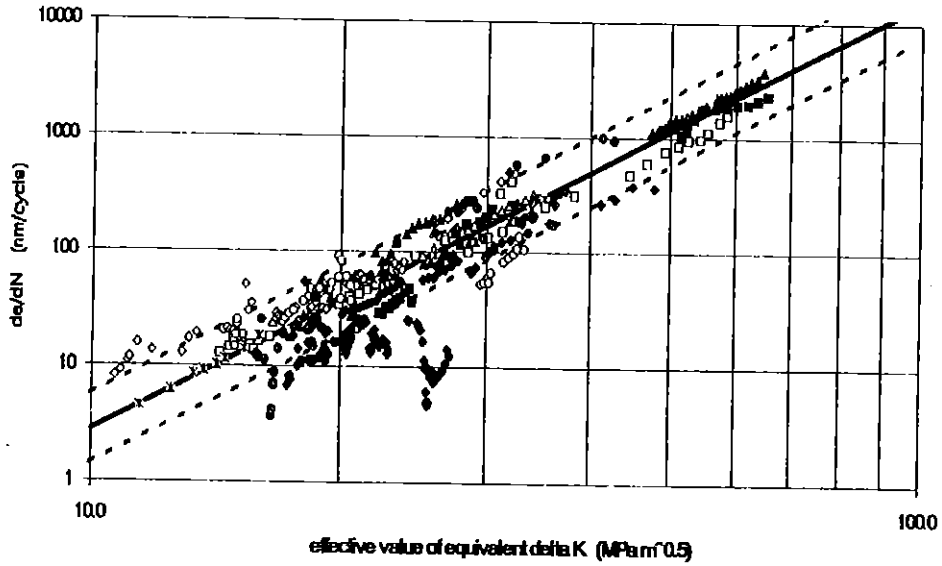

Figure 7. Correlation of coplanar fatigue crack growth data under sequential mixed-mode loading for rail steel, using the equivalent ΔK in equation (7).

model to predict coplanar fatigue crack growth in rolling contact.

In order to predict the onset of crack branching, Pineau's criterion of maximum crack growth rate is adopted (17), as cracks follow the easiest (or fastest) path available. In torsional low cycle fatigue, cracks also adopt the path that gives the greatest speed (18), either tensile or shear mode. The branch growth rate is given by equation (5), replacing the SIF range by the following formulae for Δk_I (the local SIF range for a branched crack tip). From the maximum tangential stress criterion, for the mode II shear cycle

$$\Delta k_I = 1.155\Delta K_{II} / (1 - R_{II}) + S_I \Delta K_I / (1 - R_I)$$

$$\text{or} \qquad \Delta k_I = 1.155\Delta K_{II} \qquad \text{whichever is smaller} \qquad (8)$$

and for the mode I equibiaxial cycle

$$\Delta k_I = \Delta K_I / (1 - R_I) + S_{II} 1.155\Delta K_{II} / (1 - R_{II})$$

$$\text{or} \qquad \Delta k_I = \Delta K_I \qquad \text{whichever is smaller} \qquad (9)$$

Both SIF ranges (equations (8) and (9)) contribute to the extension of branch cracks, because of the sequential nature of loading. The contributions are determined independently, then added algebraically to give overall rate, on the assumption that the

increments of extension are collinear after branching occurs. (Note that the formulation of Δk_I assumes closure at zero stress, and equibiaxial mode I stresses. Strictly collinear growth requires a zero T-stress, being the non-singular stress parallel to the crack tip.)

Prediction of rolling contact fatigue crack growth rates

Equation (5) with the equivalent SIF (equation (7)) furnishes a prediction model for coplanar crack speed, whereas equation (5) with equations (8) and (9) provides a model for branch crack growth rates. These models were applied to RCF of rails by analysing the numerical results. The numerical solution takes into account the friction generated by closure and locking on the crack faces, and therefore it generates effective ranges of SIF directly, as required for the form of the Paris law in equation (5).

Predicted crack growth rates are listed in Table 2. The ranges of SIF were determined from histories such as Fig. 4, as tabulated. Both coplanar and branch predicted rates are shown. The final two columns give the optimum propagation rate and mode of cracking, predicted by selecting the highest of the two calculated rates after Pineau's criterion.

Table 2. Predicted fatigue crack growth rates and modes.

α o	fluid	T_x kN	σ_T MPa	ΔK_I MPa$\sqrt{m}$	ΔK_{II} MPa$\sqrt{m}$	branch da/dN nm/cycle	coplanar da/dN nm/cycle	optimum crack da/dN nm/cycle	mode
15	wet	0	-200	17.0	17.6	7.1	44.6	44.6	coplanar
25	wet	0	-200	12.0	21.0	9.3	28.9	28.9	coplanar
15	wet	0	0	26.5	20.0	149.5	166.6	166.6	coplanar
15	wet	18	0	21.5	25.0	174.8	117.6	174.8	branch
25	wet	0	0	20.0	24.0	153.7	94.7	153.7	branch
15	dry	0	-200	0.0	10.5	0.1	1.1	1.1	coplanar
15	dry	18	-200	0.0	8.8	0.1	0.9	0.9	coplanar
15	dry	0	0	2.5	13.2	7.1	2.7	7.1	branch
15	dry	18	0	0.8	9.5	5.8	5.0	5.8	branch
25	dry	0	0	2.5	13.7	13.3	3.0	13.3	branch
15	dry	0	200	8.0	16.5	32.1	10.1	32.1	branch
15	dry	18	200	6.4	12.4	24.8	25.0	25.0	coplanar
25	dry	0	200	12.0	20.1	70.3	26.7	70.3	branch

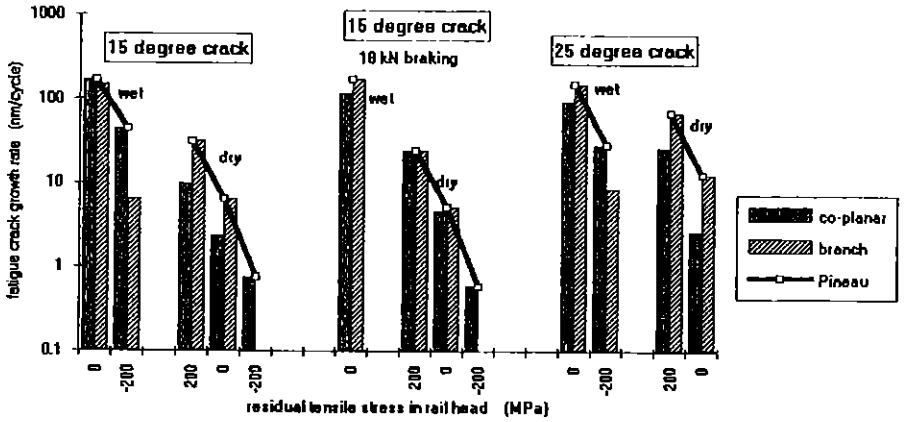

Figure 8. Prediction of growth rate and mode for various load conditions. Cracks adopt the faster rate of two calculated values, coplanar or branch (Pineau's criterion).

These predictions illustrate the effect of residual stress and two coplanar crack angles on the response of wet and dry cracks. In every case, fluid entrapment gives greater growth rates, as shown in Fig. 8. Coplanar or shallow angle cracks are observed in practice on high speed rail lines, showing stable growth until some set of conditions initiates a branch. In many cases stable branch growth without arrest is not sustainable, but occasionally growth persists to give a transverse crack that can lead to rail fracture. The conditions that encourage stable coplanar growth are i) a wet environment for fluid entrapment, ii) a shallow crack angle (15^{o} here), iii) compressive residual stress along the rail, and iv) no (braking) traction. When the crack orientation is raised to 25^{o}, branching is preferred in every case in Table 2 and Fig. 8, except when the branch is suppressed by a compressive stress in the rail head. Traction has a small effect on the growth rates. However the largest effect on propagation is the fluid entrapment itself. The acceleration of fatigue damage is illustrated in Fig. 9, where the propagation rates under wet and dry conditions are compared directly, each plotted point corresponding to fixed values of T_X, σ_r, and α. Fluid entrapment increases the growth rate obtained by an order of magnitude or more.

For the dry cracks, a friction coefficient of 0.4 was employed between the crack faces. If the sole role of the fluid was to lubricate the crack fracture surfaces, this would be best modelled by reducing the friction coefficient. An indication of the growth rates for

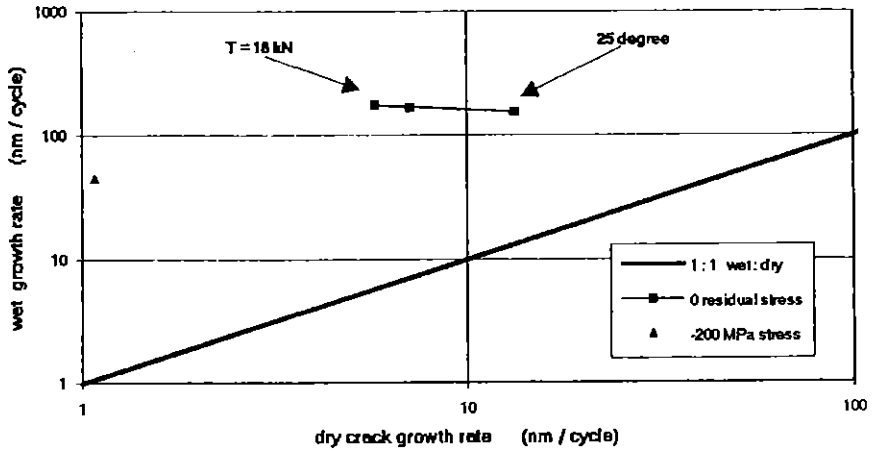

Figure 9. Comparison of wet and dry fatigue crack growth rates under sequential mixed-mode loading. Acceleration due to fluid entrapment mechanism.

lubricated crack faces (without the pressurisation of the fluid) was published previously by Bogdanski and Brown (16). Zero friction simulated the effect of full lubrication between fracture surfaces, showing that fatigue cracks were expected to branch except for shallow cracks at 25^{o} or less. However the growth rates were 2 to 10 nm/cycle, compared to speeds approaching 200 nm/cycle in Fig. 9 under fluid entrapment. As the friction was increased, the rates fell below 0.5 nm/cycle and the mode changed to coplanar.

Discussion

The predicted results are encouraging in that they comply with experience of RCF in rails. Once nucleated, cracks may branch to a mode I direction, either upwards to give surface spalling or downwards to produce a transverse fracture. The direction of branching is governed largely by the compressive residual stress in the rail head, which is superposed on the longitudinal tension in welded rails. Shallow cracks are able to grow when filled with fluid, due to the fluid entrapment mechanism which forces the crack faces apart, thereby permitting free shear displacement at the crack tip, which drives the mixed-mode coplanar mechanism.

As cracks dry out, they arrest or branch, and on branching they propagate slowly. Presumably with rain, a reversion to coplanar mode leaves a lot of small incipient branches in squats, which fail to extend as cracks become wet periodically in a temperate climate. When the coplanar crack tip falls below the surface compressive layer, branching is likely if encouraged by a dry spell. However a braking force will precipitate branching with a high growth rate, to generate a stable transverse crack.

Since wheel loads and crack angles were selected as representative values for European railways, the analysis demonstrates that "squat" RCF cracks can develop under prescribed loading conditions The integrity of rails requires that we understand the mechanisms of crack extension, and particularly the loads required for transverse cracking because such cracks can lead to fracture.

Conclusions

A model for prediction of fatigue crack growth rates in rails under rolling contact is presented. The model demonstrates that propagation of "squats" under the rail surface is feasible when a fluid entrapment mechanism is introduced, encouraging a mixed-mode shear dominated growth. However cracks may branch to a mode I direction when the residual stress, crack inclination and braking force create favourable conditions.

Acknowledgements

The authors would like to thank British Council in Warsaw and the Polish State Committee of Scientific Research (KBN) for providing financial support for this collaborative research project. The authors are indebted to the research workers in Warsaw and Sheffield who have generated the numerical solutions and the experimental results.

References

(1) Way, S., (1935), Pitting due to rolling contact, J. Applied Mech., Trans. ASME, vol. 2, pp.49-58.

(2) Bower, A.F., (1988), The influence of crack face friction and trapped fluid on surface initiated rolling contact fatigue cracks, J. Tribology, Trans. ASME, vol. 110, pp.704-711.
(3) Keer, L.M. and Bryant, M.D., (1983), A pitting model for rolling contact fatigue, J. Lubr. Technol., Trans. ASME, vol. 105, pp.198-205.
(4) Kaneta, M. & Murakami, Y., (1991), Propagation of semi-elliptical surface cracks in lubricated rolling/sliding elliptical contacts, J. Tribology, Trans. ASME, vol. 113, pp.270-275.
(5) Bogdanski, S., Olzak, M. and Stupnicki, J., (1996), Numerical stress analysis of rail rolling contact fatigue cracks, Wear, vol. 191, pp.14-24.
(6) Bogdanski, S., Olzak M. and Stupnicki, J., (1996), Influence of liquid interaction on propagation of rail rolling contact fatigue cracks, Proceedings of the 2nd mini conference on contact mechanics and wear of rail/wheel systems, (ed. I. Zobory), pp.134-143.
(7) Bogdanski, S., Olzak, M. and Stupnicki, J., (1996), The effects of face friction and tractive force on propagation of 3D 'squat' type of rolling contact fatigue crack, Proceedings of the 2nd mini conference on contact mechanics and wear of rail/wheel systems, (ed. I. Zobory), pp.164-173.
(8) Olzak, M., Stupnicki, J. and Wójcik, R (1991), Investigation of crack propagation during contact by a finite element method, Wear, vol. 146, pp.229-240.
(9) Bogdanski, S., Olzak, M. and Stupnicki, J., (1993),. An effect of internal stress and liquid pressure on crack propagation in contact area, Proceedings of the 6th international congress on tribology - Eurotrib '93, Budapest 30 Aug.-2 Sept. 1993, vol. 5, pp.310-315.
(10) Wong, S.L., Bold, P.E., Brown, M.W. and Allen, R.J., (1996), A branch criterion for shallow angled rolling contact fatigue cracks in rails, Wear, vol. 191, pp. 45-53.
(11) Bold, P.E., Brown, M.W. and Allen, R.J., (1991), Shear crack growth and rolling contact fatigue, Wear, vol.144, pp.307-317.
(12) Brown, M.W., Hemsworth, S., Wong, S.L. and Allen, R.J. (1996), Rolling contact fatigue crack growth in rail steel, Proceedings of the 2nd mini conference on contact mechanics and wear of rail/wheel systems, (ed. I. Zobory), pp.144-153.
(13) Lee, S.B., (1985), A criterion for fully reversed out-of-phase torsion and bending, Multiaxial fatigue, (eds. K.J. Miller and M.W. Brown,), ASTM STP 853, pp. 553-568.
(14) Baloch, R.A. and Brown, M.W., (1993), Crack closure analysis for the threshold of fatigue crack growth under mixed mode I/II loading, , Mixed mode fatigue and fracture, (eds. Rossmanith, H.P. and Miller, K.J.) ESIS Publication No. 14, pp.125-137.
(15) Thompson, A.W., Albert, D.E. and Gray, G.T., (1993), Fatigue crack growth in rail steels, Rail quality and maintenance for modern railway operation, (eds. J.J. Kalker, D.F. Cannon and O. Orringer), pp.361-372.
(16) Bogdanski, S. and Brown, M.W., (1997), Modelling of surface fatigue crack growth in EHD contact, Proceedings of the international conference on engineering against fatigue, Sheffield, UK, 17-21 March 1997.
(17) Hourlier, F. and Pineau, A., (1981), Fatigue crack propagation behaviour under complex mode loading, Advances in fracture research, Proceedings 5th international conference on fracture, vol. 4, pp.1841-1849.
(18) Suker, D.K.: A crack propagation approach to prediction of fatigue life and failure mode. Ph.D. thesis, University of Sheffield, 1994.